Published OnlineFirst July 27, 2017; DOI: 10.1158/1078-0432.CCR-17-0560

Cancer Therapy: Clinical

Clinical Cancer Research

T2–FLAIR Mismatch, an Imaging Biomarker for IDH and 1p/19q Status in Lower-grade Gliomas: A TCGA/TCIA Project

Sohil H. Patel[1], Laila M. Poisson[2], Daniel J. Brat[3], Yueren Zhou[2], Lee Cooper[4,5], Matija Snuderl[6], Cheddhi Thomas[6], Ana M. Franceschi[7], Brent Griffith[8], Adam E. Flanders[9], John G. Golfinos[10], Andrew S. Chi[10,11], and Rajan Jain[7,10]

Abstract

Purpose: Lower-grade gliomas (WHO grade II/III) have been classified into clinically relevant molecular subtypes based on *IDH* and 1p/19q mutation status. The purpose was to investigate whether T2/FLAIR MRI features could distinguish between lower-grade glioma molecular subtypes.

Experimental Design: MRI scans from the TCGA/TCIA lower grade glioma database ($n = 125$) were evaluated by two independent neuroradiologists to assess (i) presence/absence of homogenous signal on T2WI; (ii) presence/absence of "T2–FLAIR mismatch" sign; (iii) sharp or indistinct lesion margins; and (iv) presence/absence of peritumoral edema. Metrics with moderate–substantial agreement underwent consensus review and were correlated with glioma molecular subtypes. Somatic mutation, DNA copy number, DNA methylation, gene expression, and protein array data from the TCGA lower-grade glioma database were analyzed for molecular–radiographic associations. A separate institutional cohort ($n = 82$) was analyzed to validate the T2–FLAIR mismatch sign.

Results: Among TCGA/TCIA cases, interreader agreement was calculated for lesion homogeneity [$\kappa = 0.234$ (0.111–0.358)], T2–FLAIR mismatch sign [$\kappa = 0.728$ (0.538–0.918)], lesion margins [$\kappa = 0.292$ (0.135–0.449)], and peritumoral edema [$\kappa = 0.173$ (0.096–0.250)]. All 15 cases that were positive for the T2–FLAIR mismatch sign were *IDH*-mutant, 1p/19q non-codeleted tumors ($P < 0.0001$; PPV = 100%, NPV = 54%). Analysis of the validation cohort demonstrated substantial interreader agreement for the T2–FLAIR mismatch sign [$\kappa = 0.747$ (0.536–0.958)]; all 10 cases positive for the T2–FLAIR mismatch sign were *IDH*-mutant, 1p/19q non-codeleted tumors ($P < 0.00001$; PPV = 100%, NPV = 76%).

Conclusions: Among lower-grade gliomas, T2–FLAIR mismatch sign represents a highly specific imaging biomarker for the *IDH*-mutant, 1p/19q non-codeleted molecular subtype. *Clin Cancer Res; 23(20); 6078–85. ©2017 AACR.*

Introduction

Diffuse lower-grade gliomas (LGGs) are infiltrative brain neoplasms that include histologic classes astrocytomas, oligodendrogliomas, and oligoastrocytomas and World Health Organization (WHO) grade II and III neoplasms. Histologic classification of LGGs is limited by sampling errors during tumor biopsy or resection and more importantly suffers from high intra- and interobserver variability (1–3). In recent years, genomic analysis has dramatically improved understanding of diffuse gliomas. Several studies, including that by The Cancer Genome Atlas (TCGA) LGG Analysis Working Group, have established that LGGs can be grouped into three robust molecular classes on the basis of mutations in isocitrate dehydrogenase 1 and 2 (*IDH1* and *IDH2*, hereafter collectively referred to as *IDH*) and codeletion of chromosomes 1p and 19q (4–9). These are: (i) LGGs with *IDH* mutation and 1p/19q codeletion (*IDHmut-Codel*); (ii) LGGs with *IDH* mutation and no 1p/19q codeletion (*IDHmut-Noncodel*); and (iii) LGGs without *IDH* mutation and lacking 1p/19q codeletion (*IDH*-wild type; *IDHwt*). Among these classes, *IDHwt* neoplasms are associated with the most aggressive clinical behavior and worst outcome, similar to that of glioblastomas (WHO grade IV). *IDHmut-Codel* gliomas are associated with the most favorable

[1]Department of Radiology and Medical Imaging, University of Virginia Health System, Charlottesville, Virginia. [2]Department of Public Health, Henry Ford Health System, Detroit, Michigan. [3]Department of Pathology and Laboratory Medicine, Winship Cancer Institute at Emory University, Atlanta, Georgia. [4]Department of Biomedical Informatics, Emory School of Medicine, Atlanta, Georgia. [5]Department of Biomedical Engineering, Georgia Institute of Technology/Emory University School of Medicine, Atlanta, Georgia. [6] Department of Pathology, NYU Langone Medical Center, New York, New York. [7]Department of Radiology, NYU Langone Medical Center, New York, New York. [8]Department of Radiology, Henry Ford Health System, Detroit, Michigan. [9]Department of Radiology, Thomas Jefferson University, Philadelphia, Pennsylvania. [10]Department of Neurosurgery, NYU Langone Medical Center, New York, New York. [11]Division of Neuro-Oncology, NYU Langone Medical Center, New York, New York.

Note: Supplementary data for this article are available at Clinical Cancer Research Online (http://clincancerres.aacrjournals.org/).

Corresponding Authors: Sohil H. Patel, University of Virginia Health System, PO Box 800170, Charlottesville, VA 22908. Phone: 434-982-1736; Fax: 434-982-3880; E-mail: shp4k@virginia.edu; and Rajan Jain, New York University Langone Medical Center, 660 First Avenue, 2nd Floor, New York, NY 10016. Phone: 212-263-5219; Fax: 212-263-3838; E-mail: rajan.jain@nyumc.org

doi: 10.1158/1078-0432.CCR-17-0560

Published OnlineFirst July 27, 2017; DOI: 10.1158/1078-0432.CCR-17-0560

Translational Relevance

Among lower-grade gliomas, the presence of the T2–FLAIR mismatch sign on routine clinical MRI is highly predictive of the *IDH*-mutant 1p/19q non-codeleted glioma molecular subtype, with 100% positive predictive value. The T2–FLAIR mismatch sign is associated with a survival profile that is similar to that of the *IDH*-mutant 1p/19q non-codeleted glioma subtype and more favorable to that of *IDH*-wild-type gliomas. Conventional imaging features that distinguish between the two molecular subtypes of *IDH*-mutant glioma (1p/19q codeleted and 1p/19q non-codeleted) with high specificity are lacking, and such correlates may be clinically meaningful given the distinct prognoses between these two cohorts. Identification of this simple and robust MRI biomarker may enable a more informed pretreatment management plan and patient counsel.

clinical outcome, and possibly improved sensitivity to procarbazine, lomustine, and vincristine chemotherapy compared with non-codeleted neoplasms (10, 11). *IDHmut-Noncodel* gliomas are associated with an intermediate outcome, worse than those with 1p/19q codeletion, but far more favorable than *IDHwt* neoplasms. This molecular classification appears to capture the biologic characteristics and clinical behavior of LGGs more accurately, and with greater fidelity, than traditional histopathologic methods (4), and has been integrated into the 2016 WHO classification of brain tumors (12).

In the context of a shift toward a molecular classification of LGGs, a reappraisal of noninvasive imaging biomarkers of LGGs is warranted. Specifically, the improved molecular understanding of LGGs may advance our understanding of the various imaging phenotypes associated with LGGs. In turn, the capacity of imaging to noninvasively predict the clinical behavior of LGGs may be improved. This would have a high impact on patients with respect to treatment planning and prognostic counseling, especially in settings where detailed molecular assay of glioma specimens is not yet routinely undertaken.

The purpose of this study was to evaluate for the presence of reproducible features on conventional T2-weighted imaging (T2WI) and fluid-attenuated inversion recovery (FLAIR) MRI sequences that correlate with LGG molecular subtype and clinical outcome.

Materials and Methods

The first portion (test set) of the study was an NIH/NCI-approved retrospective review of the LGG databases of TCGA and The Cancer Imaging Archive (TCIA; ref. 13). All data in these NCI databases are anonymized and, therefore, individual institutional IRB approval is not required for this retrospective review, although it should be noted that all data were originally submitted to TCGA and TCIA by the contributing institutions under an IRB-approved protocol. TCGA LGG tumors were included in this study if they had a corresponding diagnostic MRI study in TCIA.

For the second portion of the study (validation set), IRB approval was obtained from NYU Langone Medical Center for a retrospective review of relevant patient data.

Statistical analysis was carried out utilizing R software (https://cran.r-project.org/, v 3). P values < 0.05 were considered statistically significant. False discovery rates (q) are estimated using the Benjamini–Hochberg method and reported for analysis of high-throughput molecular data.

Analysis of TCGA-LGGs (Test set)

MRI examinations were available for 199 cases of LGG in the TCIA database. Clinical information, histopathology, and molecular classifications (including *IDH* and 1p/19q-based molecular subtypes) were obtained from supplementary material from the 2016 pan-glioma paper (5, 14). Missing clinical data and progression free survival times were updated from XML files available through the TCGA data matrix (15).

Seventy-four cases were excluded: (i) MRI examination missing either T2WI or FLAIR sequence ($n = 64$); (ii) unavailable preresection MRI examination (a prior small diagnostic biopsy was not sufficient for exclusion; $n = 7$); (iii) infratentorial location of LGG ($n = 1$); (iv) LGG was excluded from TCGA ($n = 1$); and (v) *IDH* and 1p/19q status was unavailable ($n = 1$). A total of 125 TCGA-profiled LGGs were ultimately included for this analysis.

MRI examinations were analyzed by two independent neuroradiologists with 17 and 3 years of experience, respectively. Both readers have been certified by the American Board of Radiology in both Diagnostic Radiology and also the subspecialty of Neuroradiology. The readers reviewed the cases blinded to the histopathologic diagnosis, molecular classification, and patient outcome.

Readers evaluated the T2WI and FLAIR sequences of each MRI examination. They determined the following characteristics of the LGGs, using a binary scoring system for each: (i) presence or absence of homogenous signal intensity on T2WI; (ii) presence or absence of complete/near-complete hyperintense signal on T2WI, and relatively hypointense signal on FLAIR except for a hyperintense peripheral rim ("T2–FLAIR mismatch"; Fig. 1); (iii) margins of lesion sharp or indistinct; and (iv) presence or absence of peritumoral edema.

After independent data collection, interreader agreement was calculated using the κ coefficient (κ; "irr" package). $0 \leq \kappa \leq 0.2$ indicated slight agreement, $0.2 < \kappa \leq 0.4$ indicated fair agreement, $0.4 < \kappa \leq 0.6$ indicated moderate agreement, and $\kappa > 0.6$ indicated substantial agreement. Discordant results were resolved by consensus for the imaging characteristics which demonstrated moderate or substantial interreader agreement.

Analysis of NYU-LGGs (Validation set)

On the basis of the results obtained from analyzing LGGs in the TCGA/TCIA database, a separate analysis of LGGs in patients who were managed at our institution (NYU Langone Medical Center) was subsequently undertaken for the purpose of validating the T2–FLAIR mismatch sign only.

LGG cases were derived from an internal database maintained by the Neuropathology department in our institution. One hundred and fifteen LGGs accrued from the years 2011 to 2014 were eligible for analysis. Thirty-three cases were excluded: pediatric patients ($n = 22$); no available preoperative imaging ($n = 8$); infratentorial location of LGG ($n = 2$); no available pathologic data ($n = 1$). Eighty two cases had preoperative MRI scans with both T2WI and FLAIR sequences, histopathologic diagnosis, and WHO grading, and were included for analysis.

Published OnlineFirst July 27, 2017; DOI: 10.1158/1078-0432.CCR-17-0560

Preoperative MRI scans of these cases were analyzed by the two neuroradiologist readers, who were blinded to the histopathologic diagnosis, molecular classification, and patient outcome. Readers evaluated T2WI and FLAIR sequences to determine the presence or absence of the T2–FLAIR mismatch sign. After independent data collection, interreader agreement was calculated, and discordant results were resolved by consensus.

Histopathologic grading

For TCGA/TCIA cohort, histology and grading of tissues submitted to TCGA were confirmed by neuropathology review, as previously described (4, 5). For the NYU (validation) cohort, the histopathologic diagnosis and WHO grade were ascertained from the electronic medical record.

In addition, an independent neuropathologist performed a blinded review of histopathologic specimens of 30 *IDHmut-Noncodel* LGGs from the TCGA/TCIA cohort, 15 positive and 15 negative for the T2–FLAIR mismatch sign. Specimens were assessed for cellularity, edema, hemosiderin, microcysts, mucin, vacuolization, and vessel alterations. Tissue samples were of variable quality and consistency, including some cases associated with a single available slide.

Molecular classification and analysis

Molecular classification for TCGA/TCIA cohort was derived from the 2016 pan-glioma paper (5) and includes (a) somatic mutation in the isocitrate dehydrogenase genes (*IDH1* or *IDH2*), from whole-exome sequencing, (b) codeletion of chromosomal arms 1p and 19q, from Affymetrix SNP6.0 arrays, and (c) the seven methylation specific classes defined for *IDH*-mutated tumors (Codel, G-CIMP-high, G-CIMP-low) and *IDH* wild-type tumors (classic-like, mesenchymal-like, LGm6-GBM, and PA-like LGG). Categorical association between consensus MRI metrics and molecular subtype was determined using Fisher exact test for 2×2 tables.

A grid plot of genomic alterations (16, 17) was generated for the TCGA cohort, focusing on glioma-specific somatic mutations and copy-number variants (4). The total number of alterations in this gene set was compared between groups by the Wilcoxon rank-sum test. MRNA sequencing profiles for 125 cases were obtained from the Broad Institute TCGA Genome Data Analysis Center (18). Gene set enrichment analysis (GSEA) was performed using the differential expression ranking metric (19). We analyzed pathways from the NCI/Nature Pathway Interaction Database obtained from MSigDB (19, 20). Family-wise error rate (FWER) is reported to account for multiple comparisons. Total protein and phosphoprotein levels, measured by reverse phase protein array (RPPA), were obtained from the Broad Institute TCGA Genome Data Analysis Center (18). Differences between groups were assessed by two-sample *t* tests. The Core Analysis of Ingenuity Pathway Analysis software was conducted on lists of differential genes found by RNAseq or RPPA data.

For the NYU (validation) cohort, 1p/19q status and *IDH* status were retrieved from the electronic medical record. Both markers were tested in a Clinical Laboratory Improvement Amendments–certified NYU molecular pathology laboratory. 1p/19q was tested using PCR loss of heterozygosity. *IDH* status was first screened by *IDH1 R132H* mutant specific clinically validated antibody (21, 22). In negative cases, *IDH* mutation status was assessed by a clinically validated IonTorrent targeted next-generation sequencing panel (23, 24).

Survival analysis

Overall survival and progression-free survival curves for the TCGA/TCIA cohort were constructed by Kaplan–Meier estimation, and log-rank tests were used to compare survival curves segregated by MRI metrics, Age-adjusted survival estimates were generated using Cox proportional hazards regression modeling. Analyses were performed in R using the "survival" package.

Results

Analysis of TCGA-LGGs (Test set)

Table 1 displays characteristics of the 125 LGGs from the TCGA/TCIA cohort. Further refinement by DNA methylation profiles yielded 37 Codel, 62 G-CIMP-high, and 3 G-CIMP-low among the *IDH*-mutant tumors, and 14 mesenchymal-like, six classic-like, three PA-like gliomas among the *IDHwt* tumors.

Independent MRI analysis revealed interreader agreement measurements for lesion homogeneity [$\kappa = 0.234$ (0.111–0.358)], T2–FLAIR mismatch sign [$\kappa = 0.728$ (0.538–0.918)], lesion margins [$\kappa = 0.292$ (0.135–0.449)], and peritumoral edema [$\kappa = 0.173$ (0.096–0.250)]. Discordant cases with respect to the T2–FLAIR mismatch sign were resolved in consensus, and the readers determined that the T2–FLAIR mismatch sign was present in 15 cases (12%) and absent in 110 cases (88%; Figs. 1 and 2). Consensus review was not undertaken for the other imaging metrics due to low levels of interreader agreement. Reader results are displayed in Supplementary Table S1.

Among the 15 cases with positive T2–FLAIR mismatch sign, tumor histology included six astrocytomas, six oligodendrogliomas, and three oligoastrocytomas (of note, designation of "oligoastrocytoma" was assigned in our cohort based on prior WHO classification, and is discouraged based on the 2016 WHO classification). There were 11 grade II and 4 grade III lesions. All 15 cases with a positive T2–FLAIR mismatch sign were *IDHmut-Noncodel* neoplasms. The T2–FLAIR mismatch sign was significantly associated with *IDHmut-Noncodel* molecular subtype ($P < 0.0001$). The T2–FLAIR mismatch sign as a marker of the *IDHmut-Noncodel* subtype showed a positive predictive value (PPV) of 100% and a negative predictive value (NPV) of 54%. Table 2 displays the distribution of LGGs by histopathologic assignment and the T2–FLAIR mismatch sign, and Table 3 displays the distribution of LGGs by molecular subtype and the T2–FLAIR mismatch sign. Of the 15 T2–FLAIR mismatch positive gliomas, 10 harbored *IDH1*-R132H mutations and five harbored other *IDH* mutations, including three *IDH1*-R132S mutations, one *IDH1*-R132W mutation, and one *IDH1*-R132C mutation. With respect to DNA methylation subtype, all 15 LGGs with positive T2–FLAIR mismatch were G-CIMP-high.

Analysis of LGGs from the NYU database (validation set)

Table 1 displays the clinical characteristics of the 82 LGGs from the NYU cohort.

Interreader agreement for the assessment of the T2–FLAIR mismatch was substantial [$\kappa = 0.747$ (0.536–0.958)]. After resolving discordant cases in consensus, the readers determined that the T2–FLAIR mismatch sign was present in 10 cases (12%) and absent in 72 cases (88%).

Published OnlineFirst July 27, 2017; DOI: 10.1158/1078-0432.CCR-17-0560

Table 1. Characteristics of the study populations, including histology and molecular subtype of the LGGs, patient age at diagnosis, and gender. Count and percentage are provided for categorical variables

	TCGA cases (test set) ($n = 125$)	NYU cases (validation set) ($n = 82$)
Histology		
Astrocytoma		
Grade II	8 (6%)	12 (15%)
Grade III	30 (24%)	28 (34%)
Oligodendroglioma		
Grade II	33 (26%)	22 (27%)
Grade III	21 (17%)	16 (20%)
Oligoastrocytoma		
Grade II	17 (14%)	1 (1%)
Grade III	16 (13%)	3 (4%)
Molecular subtype		
IDHmut-Codel	34 (27%)	31 (52%)[a]
IDHmut-Noncodel	68 (54%)	22 (37%)[a]
IDHwt	23 (18%)	7 (12%)[a]
Age at diagnosis (years)		
Median	45.5	45
Range	20–75	21–82
Gender		
Female	63 (50%)	38 (46%)
Male	62 (50%)	44 (54%)

[a]Molecular subtype was available for a total of 60 cases among the NYU cohort.

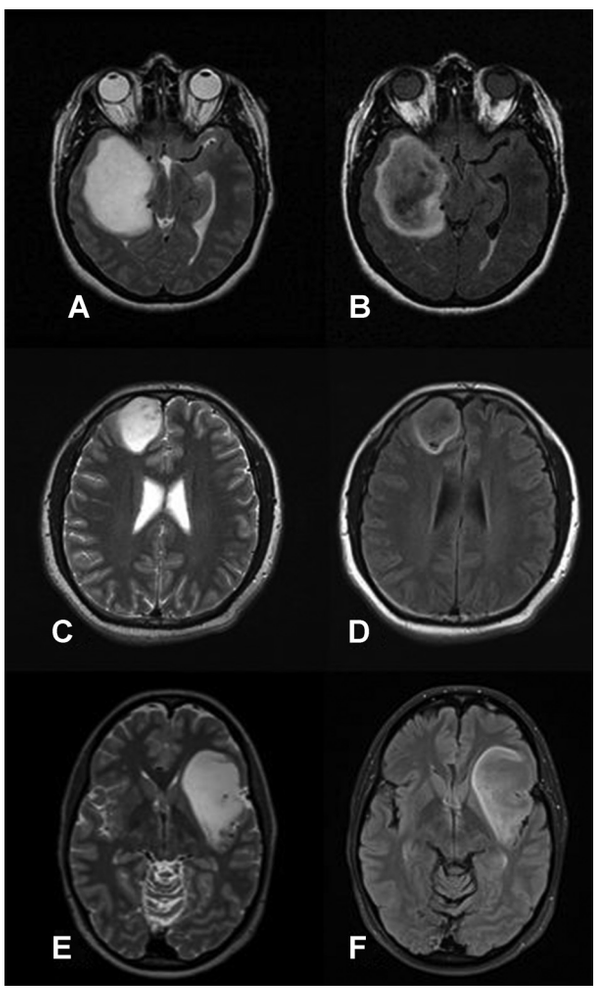

Among 10 cases with a positive T2–FLAIR mismatch sign, tumor histology included six astrocytomas, three oligodendrogliomas, and one oligoastrocytoma. There were five WHO grade II and five WHO grade III lesions. *IDH* and 1p/19q status was available in all of the positive T2–FLAIR mismatch cases; all 10 of these cases were *IDHmut-Noncodel* lesions. The T2–FLAIR mismatch sign was significantly associated with the *IDHmut-Noncodel* molecular subtype ($P < 0.00001$; PPV = 100%, NPV = 76%). Of the 10 T2–FLAIR mismatch positive gliomas, eight harbored *IDH1*-R132H mutations and two harbored other *IDH* mutations, including one *IDH1*-R132L mutation, and one *IDH1*-R132C mutation. Table 2 displays the distribution of LGGs by histopathologic assignment and the T2–FLAIR mismatch sign, and Table 3 displays the distribution of LGGs by molecular subtype and the T2–FLAIR mismatch sign.

Exploratory T2–FLAIR mismatch sign correlates

Genomic alteration profile of LGGs differentiated by the T2–FLAIR mismatch sign showed no significant differences between the groups in rates of mutation or genomic alteration overall when the analysis included all 125 LGGs in the cohort ($P = 0.18$ and $P = 0.27$, respectively) and also when the analysis was restricted to *IDHmut-Noncodel* LGGs ($P = 0.73$ and $P = 0.91$, respectively).

Gene expression profile analysis of the 125 LGGs in our TCGA/TCIA cohort using GSEA identified the mTOR pathway as highly enriched with genes upregulated in mRNA profiles of the positive T2–FLAIR mismatch cases ($P = 0.01$, FWER = 0.695). Among the genes most significantly upregulated in positive T2–FLAIR mismatch mRNA profiles are *NRAS* (98.8%-tile), *RAF1* (92.7 %-tile), *MTOR* (96.8 %-tile), *RICTOR* (98.5 %-tile), and *RPTOR* (81.7 %-tile). All of these genes were in the core set found in the mTOR pathway leading-edge analysis. These results were not reproduced when we restricted our analysis to *IDHmut-Noncodel* neoplasms alone (Supplementary Tables S2 and S3).

Proteomic analysis of the 125 LGGs in the TCGA/TCIA cohort using RPPA revealed increased levels of proteins in the mTOR signaling pathway among the positive T2–FLAIR mismatch cases, including mTOR ($P < 0.0001$, adj $P = 0.004$), RPTOR ($P = 0.02$, adj $P = 0.3$), and RICTOR ($P = 0.03$, adj $P = 0.4$). Decreased levels of erbB-2 ($P < 0.0001$, adj $P = 0.007$) were also noted among the positive T2–FLAIR mismatch cases. When the RPPA was restricted only to *IDHmut-Noncodel* neoplasms, mTOR ($P = 0.002$, adj $P = 0.3$), RICTOR ($P = 0.04$, adj $P = 0.7$), and RPTOR ($P = 0.04$, adj $P = 0.7$) remained increased among the positive T2–FLAIR mismatch cases, as were several proteins in the AMPK signaling pathway (FOXO3, MET, FASN, ACACA, and mTOR; Supplementary Tables S4 and S5).

Figure 1.
Three cases of *IDHmut-Noncodel* LGGs that were positive for the T2–FLAIR mismatch sign. **A** and **B,** Patient TCGA-DU-6407 from the TCIA database with a right temporal lobe glioma. **C** and **D,** Patient TCGA-EZ-7265A from the TCIA database with a right frontal lobe glioma. **E** and **F**, patient from the NYU database with a left insular glioma. The T2WI (**A**, **C**, and **E**), demonstrates complete or near-complete hyperintense signal throughout the lesions. On the FLAIR sequences (**B**, **D**, and **F**, the lesions display relatively hypointense signal throughout the majority of the lesion when compared with T2WI, with the exception of a peripheral rim of hyperintense signal.

Published OnlineFirst July 27, 2017; DOI: 10.1158/1078-0432.CCR-17-0560

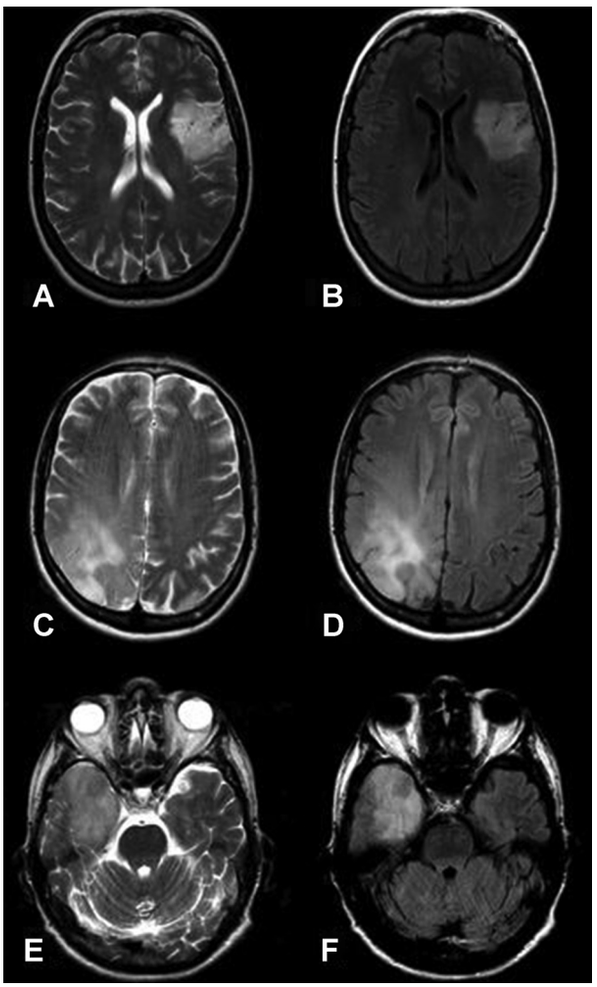

Figure 2.

Three cases that were negative for the T2–FLAIR mismatch sign. **A** and **B,** Patient TCGA-CS-6668 from the TCIA database with a left insular/frontal *IDHmut-Codel* glioma. **C** and **B,** patient TCGA-CS-6665 from the TCIA database with a right parietal *IDHmut-Noncodel* glioma. **E** and **F,** Patient from the NYU database with a right temporal lobe *IDHwt* glioma. T2WI (**A**, **C**, and **E**) and FLAIR (**B**, **D**, and **F**) sequences are depicted for each lesion.

Histopathologic analysis of 30 *IDHmut-Noncodel* neoplasms from the TCGA/TCIA cohort revealed no feature that was significantly different between the T2–FLAIR mismatch positive and T2–FLAIR mismatch negative cases. There was a nonsignificant trend for the presence of abundant microcysts in the T2–FLAIR mismatch positive cases compared with the T2–FLAIR mismatch negative cases ($P = 0.128$). In the slides that were available for review in the TCGA/TCIA cohort, 11 out of 15 T2–FLAIR mismatch positive cases contained regions composed of numerous, confluent, variably-sized microcystic spaces with only modest intervening neuropil (Supplementary Fig. S1). However, our finding did not reach statistical significance and larger T2–FLAIR mismatch positive cohorts will be required for confirmation.

The median progression-free survival and overall survival of T2–FLAIR mismatch positive gliomas were 38.9 months (30.0–indeterminate) and 65.7 months (43.9–indeterminate), respectively. There were insufficient data to calculate the upper bound of 95% confidence intervals. No significant difference in progression-free survival or overall survival was detected between positive and negative T2–FLAIR mismatch cases when analyzing all of the cases from the TCGA/TCIA cohort, however, this comparison is dependent upon the relative proportion of *IDH*-mutant and *IDHwt* gliomas within the cohort. Further survival analysis was undertaken in the *IDHmut-Noncodel* subset alone (which contained all positive T2–FLAIR mismatch cases), and here also there was no significant difference in survival times between positive and negative T2–FLAIR mismatch cases. The median survival times associated with T2–FLAIR mismatch positive gliomas are similar to established outcomes in *IDHmut-Noncodel* gliomas, reflecting the molecular subtype that the T2–FLAIR mismatch sign specifically identifies (Supplementary Fig. S2).

Discussion

Our results indicate that, among LGGs, the T2–FLAIR mismatch sign represents a highly specific marker for the *IDHmut-Noncodel* molecular subtype of *IDH*-mutant gliomas, with 100% PPV in both the test and validation sets. Among the imaging metrics assessed in this study, the T2–FLAIR mismatch sign showed a uniquely high level of interreader agreement. Imaging correlates that distinguish between the two *IDH*-mutant glioma molecular subtypes (1p/19q codeleted and 1p/19q non-codeleted) with high specificity are lacking, and an additional molecular test to interrogate the 1p/19q status is currently required. Development of a robust noninvasive biomarker that can distinguish between these two prognostically distinct *IDH*-mutant glioma subtypes could assist in the diagnostic evaluation and initial management of these patients.

Multiple recent studies have also attempted to correlate MRI features of gliomas with underlying molecular status. For example, frontal lobe and non-midline tumor locations are more frequent in *IDH*-mutant lesions (4, 25, 26). *IDH*-mutant lesions

Table 2. LGGs from the TCGA/TCIA and NYU databases distributed by histopathologic assignment and the presence or absence of the T2–FLAIR mismatch sign

	TCGA/TCIA cases ($n = 125$)		NYU cases ($n = 82$)	
	Positive T2–FLAIR mismatch	Negative T2–FLAIR mismatch	Positive T2–FLAIR mismatch	Negative T2–FLAIR mismatch
Astrocytoma grade II	3	5	2	10
Astrocytoma grade III	3	27	4	24
Oligodendroglioma grade II	6	27	3	19
Oligodendroglioma grade III	0	21	0	16
Oligoastrocytoma grade II	2	15	0	1
Oligoastrocytoma grade III	1	15	1	2
Total	15	110	10	72

Table 3. LGGs from the TCGA/TCIA and NYU databases distributed by molecular subtype and the presence or absence of the T2–FLAIR mismatch sign

	TCGA/TCIA cases ($n = 125$)		NYU cases ($n = 60$)[a]	
	Positive T2–FLAIR mismatch	Negative T2–FLAIR mismatch	Positive T2–FLAIR mismatch	Negative T2–FLAIR mismatch
IDHmut-Codel	0	34	0	31
IDHmut-Noncodel	15	53	10	12
IDHwt	0	23	0	7
Total	15	110	10	50

[a]The 60 NYU cases with available molecular data are included in this table.

also more frequently display sharp margins, homogenous internal signal intensity, and lesser degree of contrast enhancement when compared with *IDH*-wild type lesions (26–28). *IDHmut-Codel* and *IDHmut-Noncodel* gliomas appear to differ with respect to tumor margins and internal heterogeneity (29). Nonetheless, it is generally accepted that conventional MRI findings do not possess sufficient specificity to predict the underlying histologic or molecular subtype of an LGG in an individual patient (30). In contrast, our results introduce a simple imaging feature which appears to be highly specific for underlying molecular status (although this feature is of low sensitivity). We know of no conventional MRI feature that possesses as high a level of specificity in predicting underlying *IDH* and 1p/19q status as appears to be the case for the T2–FLAIR mismatch sign.

Advanced MRI techniques such as perfusion-weighted imaging (31–33), MR-spectroscopy (34–36), and sodium-imaging (37) have also revealed differences between *IDH*-mutant and wild-type neoplasms. Among these advanced techniques, the most promising appears to be 2-hydroxyglutarate (2HG) detection utilizing proton MR-spectroscopy. Detection of 2HG is a highly specific marker for underlying *IDH* mutation. Unfortunately, 2HG detection with MR-spectroscopy is a significant technical challenge due to spectral overlap of 2HG with background metabolites, and is not yet a standardized and routinely performed imaging sequence in most clinical practices. Moreover, it does not predict the 1p/19q status of gliomas.

Our finding that the T2–FLAIR mismatch sign identifies a molecular subset of gliomas (100% PPV for *IDHmut-Noncodel*) with a far more favorable survival profile than *IDHwt* glioma (in keeping with the well-known fact that *IDH*-mutant gliomas are far more indolent than *IDHwt* gliomas (4, 6, 8, 38–41)) might provide useful information to clinicians during the initial management of patients. Unambiguous radiographic evidence that a glioma is *IDH*-mutant and, therefore, a relatively favorable subtype would assist patient counsel. Moreover, recent studies indicate that patients with *IDH*-mutant gliomas significantly benefit from gross total tumor resection compared with partial resection (42), and the survival benefit achieved with gross total resection may have greater impact in the *IDHmut-Noncodel* subset (43). Therefore, the T2–FLAIR mismatch sign might provide useful information for the neurosurgeon prior to glioma resection. Although surgery should be as extensive as safely possible, regardless of *IDH* mutation status, a surgeon may be willing to extend further (e.g., supplementary motor area) if it is known that a tumor is *IDH* mutant.

Our study attempted to assess imaging features besides the T2–FLAIR mismatch sign. These included imaging features related to internal signal texture (homogenous or inhomogeneous), tumor margin characteristics (sharp or indistinct), and presence/absence of peritumoral edema, that have in prior studies been correlated with histologic and molecular class as well as the clinical behavior of gliomas (27, 44–46). However, the interreader agreement for each of these metrics was poor in our study. It should be noted that the readers in our study assessed all metrics in a qualitative and binary manner, one which we thought was most directly applicable to clinical neuroradiology practice. Prior studies assessing some of these imaging metrics have instead used quantitative and semi-quantitative methods that allowed for a graded assessment of tumor characteristics. It is possible that the T2–FLAIR mismatch sign showed such high interreader agreement due to its fairly striking and characteristic imaging appearance, one that conforms readily to a binary (yes/no) scoring system.

To our knowledge, a version of the T2–FLAIR mismatch sign in glioma has only been reported once previously. In a case series of protoplasmic astrocytomas, Tay and colleagues reported that all cases showed at least partial "suppression" of FLAIR signal relative to the signal on T2WI (47). Protoplasmic astrocytomas are rare WHO grade II diffuse gliomas which typically affect young adults and follow a relatively indolent course (48). Therefore, it is likely that this case series was largely composed of *IDH*-mutant tumors (even though the study belongs to premolecular classification era and does not mention molecular analysis). The MRI figures displayed in their article strongly resemble the appearance of the T2–FLAIR mismatch sign reported in our study.

It is unclear why only some, but not all, *IDHmut-Noncodel* lesions manifest the T2–FLAIR mismatch sign. One possibility is that the T2–FLAIR mismatch sign identifies some as-yet undiscovered molecular subgroup within the *IDHmut-Noncodel* class. In our exploratory RPPA analysis, tumors in the *IDHmut-Noncodel* class showed significantly increased levels of proteins in the mTOR pathway among the positive T2–FLAIR mismatch cases, including mTOR, RICTOR, and RPTOR. The GSEA also revealed increased expression of genes in the mTOR pathway among T2–FLAIR mismatch positive cases (though only when the analysis included all cases from our cohort). Several recent studies showed *IDH*-mutant gliomas frequently acquire activating mutations in the mTOR pathway at progression (49–51). However, our findings remain preliminary and whether mTOR is activated in a subset of *IDH*-mutant gliomas requires validation.

Our study has several limitations. It followed a retrospective design, and the results would benefit from prospective validation. However, our usage of the publically available TCGA/TCIA database readily permits other groups to reanalyze this data and independently verify our results. Our study utilized subjective MRI interpretation by two readers of variable experience, rather than quantitative or semi-quantitative image analysis. Although in theory, this might limit the reproducibility of our results, our analysis utilized routinely available MR imaging sequences (T2WI, FLAIR) and the assessment of relatively simple imaging features, potentially permitting wide clinical applicability and

more straightforward future validation efforts compared with more technically demanding and investigational MRI sequences. Finally, although the T2–FLAIR mismatch sign appears to represent a highly specific sign of *IDH*-mutant lesions among LGGs, its specificity amongst all possible brain neoplasms cannot be ascertained based on our data.

Conclusion

Among LGGs, the T2–FLAIR mismatch sign represents a highly specific noninvasive imaging biomarker for the *IDHmut-Noncodel* molecular subclass of *IDH*-mutant glioma. This simple and robust MRI biomarker can be identified using standard clinical MRI techniques and may enable a more informed pretreatment management plan and patient counsel.

Disclosure of Potential Conflicts of Interest

L. Cooper reports receiving speakers bureau honoraria from Varian Medical Systems. No potential conflicts of interest were disclosed by the other authors.

Authors' Contributions

Conception and design: S.H Patel, L.M. Poisson, R. Jain
Development of methodology: S.H Patel, M. Snuderl, R. Jain
Acquisition of data (provided animals, acquired and managed patients, provided facilities, etc.): S.H Patel, D.J. Brat, C. Thomas, A.M. Franceschi, J.G. Golfinos, R. Jain
Analysis and interpretation of data (e.g., statistical analysis, biostatistics, computational analysis): S.H Patel, L.M. Poisson, D.J. Brat, Y. Zhou, L. Cooper, M. Snuderl, C. Thomas, A.S. Chi, R. Jain
Writing, review, and/or revision of the manuscript: S.H Patel, L.M. Poisson, D.J. Brat, L. Cooper, M. Snuderl, A.M. Franceschi, B. Griffith, J.G. Golfinos, A.S. Chi, R. Jain, A. Flanders
Administrative, technical, or material support (i.e., reporting or organizing data, constructing databases): S.H Patel, A.M. Franceschi, R. Jain
Study supervision: S.H Patel, R. Jain

Grant Support

L. Cooper received financial support from National Cancer Institute grant U24CA194362. The remaining authors received no financial support for their contributions to this article.

The costs of publication of this article were defrayed in part by the payment of page charges. This article must therefore be hereby marked *advertisement* in accordance with 18 U.S.C. Section 1734 solely to indicate this fact.

Received February 24, 2017; revised May 11, 2017; accepted July 19, 2017; published OnlineFirst July 27, 2017.

References

1. Coons SW, Johnson PC, Scheithauer BW, Yates AJ, Pearl DK. Improving diagnostic accuracy and interobserver concordance in the classification and grading of primary gliomas. Cancer 1997;79:1381–93.
2. van den Bent MJ. Interobserver variation of the histopathological diagnosis in clinical trials on glioma: a clinician's perspective. Acta Neuropathol 2010;120:297–304.
3. Siegal T. Clinical relevance of prognostic and predictive molecular markers in gliomas. Advances and technical standards in neurosurgery. 43. Switzerland: Springer International Publishing; 2016. p. 91–108.
4. Cancer Genome Atlas Research N, Brat DJ, Verhaak RG, Aldape KD, Yung WK, Salama SR, et al. Comprehensive, integrative genomic analysis of diffuse lower-grade gliomas. N Engl J Med 2015;372:2481–98.
5. Ceccarelli M, Barthel FP, Malta TM, Sabedot TS, Salama SR, Murray BA, et al. Molecular profiling reveals biologically discrete subsets and pathways of progression in diffuse glioma. Cell 2016;164:550–63.
6. Eckel-Passow JE, Lachance DH, Molinaro AM, Walsh KM, Decker PA, Sicotte H, et al. Glioma groups based on 1p/19q, IDH, and TERT promoter mutations in tumors. N Engl J Med 2015;372:2499–508.
7. Suzuki H, Aoki K, Chiba K, Sato Y, Shiozawa Y, Shiraishi Y, et al. Mutational landscape and clonal architecture in grade II and III gliomas. Nat Genet 2015;47:458–68.
8. Jiao Y, Killela PJ, Reitman ZJ, Rasheed AB, Heaphy CM, de Wilde RF, et al. Frequent ATRX, CIC, FUBP1 and IDH1 mutations refine the classification of malignant gliomas. Oncotarget 2012;3:709–22.
9. Killela PJ, Reitman ZJ, Jiao Y, Bettegowda C, Agrawal N, Diaz LA Jr., et al. TERT promoter mutations occur frequently in gliomas and a subset of tumors derived from cells with low rates of self-renewal. Proc Natl Acad Sci U S A 2013;110:6021–6.
10. Cairncross G, Wang M, Shaw E, Jenkins R, Brachman D, Buckner J, et al. Phase III trial of chemoradiotherapy for anaplastic oligodendroglioma: long-term results of RTOG 9402. J Clin Oncol 2013;31:337–43.
11. van den Bent MJ, Brandes AA, Taphoorn MJ, Kros JM, Kouwenhoven MC, Delattre JY, et al. Adjuvant procarbazine, lomustine, and vincristine chemotherapy in newly diagnosed anaplastic oligodendroglioma: long-term follow-up of EORTC brain tumor group study 26951. J Clin Oncol 2013;31:344–50.
12. Louis DN, Perry A, Reifenberger G, von Deimling A, Figarella-Branger D, Cavenee WK, et al. The 2016 world health organization classification of tumors of the central nervous system: a summary. Acta Neuropathol 2016;131:803–20.
13. The Cancer Imaging Archive. https://public.cancerimagingarchive.net/ncia/login.jsf. Accessed April 2016.
14. The Cancer Genome Atlas. Supplemental material from doi:10.1016. https://tcga-data.nci.nih.gov/docs/publications/lgggbm_2016/. Accessed April 2016.
15. The Cancer Genome Atlas. Data Matrix. https://gdc.cancer.gov/. Accessed April 2016.
16. Cerami E, Gao J, Dogrusoz U, Gross BE, Sumer SO, Aksoy BA, et al. The cBio cancer genomics portal: an open platform for exploring multidimensional cancer genomics data. Cancer Discov 2012;2:401–4.
17. Gao J, Aksoy BA, Dogrusoz U, Dresdner G, Gross B, Sumer SO, et al. Integrative analysis of complex cancer genomics and clinical profiles using the cBioPortal. Sci Signal 2013;6:pl1.
18. Broad Institute TCGA Genome Data Analysis Center (2016): Firehouse stddata 2016 01 28 run. Broad Institute of MIT and Harvard. doi: 10.7908/C11G0KM9.
19. Subramanian A, Tamayo P, Mootha VK, Mukherjee S, Ebert BL, Gillette MA, et al. Gene set enrichment analysis: a knowledge-based approach for interpreting genome-wide expression profiles. Proc Natl Acad Sci U S A 2005;102:15545–50.
20. Schaefer CF, Anthony K, Krupa S, Buchoff J, Day M, Hannay T, et al. PID: the pathway interaction database. Nucleic Acids Res 2009;37:D674–9.
21. Capper D, Weissert S, Balss J, Habel A, Meyer J, Jager D, et al. Characterization of R132H mutation-specific IDH1 antibody binding in brain tumors. Brain Pathol 2010;20:245–54.
22. Capper D, Zentgraf H, Balss J, Hartmann C, von Deimling A. Monoclonal antibody specific for IDH1 R132H mutation. Acta Neuropathol 2009;118:599–601.
23. Dubbink HJ, Atmodimedjo PN, Kros JM, French PJ, Sanson M, Idbaih A, et al. Molecular classification of anaplastic oligodendroglioma using next-generation sequencing: a report of the prospective randomized EORTC Brain Tumor Group 26951 phase III trial. Neuro-Oncology 2016;18:388–400.
24. Zacher A, Kaulich K, Stepanow S, Wolter M, Kohrer K, Felsberg J, et al. Molecular diagnostics of gliomas using next generation sequencing of a glioma-tailored gene panel. Brain Pathol 2017;27:146–59.
25. Sun ZL, Chan AK, Chen LC, Tang C, Zhang ZY, Ding XJ, et al. TERT promoter mutated WHO grades II and III gliomas are located preferentially in the frontal lobe and avoid the midline. Int J Clin Exp Pathol 2015;8:11485–94.

26. Lai A, Kharbanda S, Pope WB, Tran A, Solis OE, Peale F, et al. Evidence for sequenced molecular evolution of IDH1 mutant glioblastoma from a distinct cell of origin. J Clin Oncol 2011;29:4482–90.
27. Qi S, Yu L, Li H, Ou Y, Qiu X, Ding Y, et al. Isocitrate dehydrogenase mutation is associated with tumor location and magnetic resonance imaging characteristics in astrocytic neoplasms. Oncol Lett 2014;7: 1895–902.
28. Reyes-Botero G, Dehais C, Idbaih A, Martin-Duverneuil N, Lahutte M, Carpentier C, et al. Contrast enhancement in 1p/19q-codeleted anaplastic oligodendrogliomas is associated with 9p loss, genomic instability, and angiogenic gene expression. Neuro-oncology 2014;16:662–70.
29. Johnson DR, Diehn FE, Giannini C, Jenkins RB, Jenkins SM, Parney IF, et al. Genetically defined oligodendroglioma is characterized by indistinct tumor borders at MRI. AJNR Am J Neuroradiol 2017;38:678–84.
30. Upadhyay N, Waldman AD. Conventional MRI evaluation of gliomas. Br J Radiol 2011;84:S107–11.
31. Jain R, Poisson L, Narang J, Gutman D, Scarpace L, Hwang SN, et al. Genomic mapping and survival prediction in glioblastoma: molecular subclassification strengthened by hemodynamic imaging biomarkers. Radiology 2013;267:212–20.
32. Jain R, Poisson L, Narang J, Scarpace L, Rosenblum ML, Rempel S, et al. Correlation of perfusion parameters with genes related to angiogenesis regulation in glioblastoma: a feasibility study. AJNR Am J Neuroradiol 2012;33:1343–8.
33. Kickingereder P, Sahm F, Radbruch A, Wick W, Heiland S, Deimling A, et al. IDH mutation status is associated with a distinct hypoxia/angiogenesis transcriptome signature which is non-invasively predictable with rCBV imaging in human glioma. Sci Rep 2015;5:16238.
34. de la Fuente MI, Young RJ, Rubel J, Rosenblum M, Tisnado J, Briggs S, et al. Integration of 2-hydroxyglutarate-proton magnetic resonance spectroscopy into clinical practice for disease monitoring in isocitrate dehydrogenase-mutant glioma. Neuro-oncology 2016;18:283–90.
35. Kim H, Kim S, Lee HH, Heo H. In-Vivo proton magnetic resonance spectroscopy of 2-hydroxyglutarate in isocitrate dehydrogenase-mutated gliomas: a technical review for neuroradiologists. Korean J Radiol 2016; 17:620–32.
36. Andronesi OC, Kim GS, Gerstner E, Batchelor T, Tzika AA, Fantin VR, et al. Detection of 2-hydroxyglutarate in IDH-mutated glioma patients by in vivo spectral-editing and 2D correlation magnetic resonance spectroscopy. Sci Translat Med 2012;4:116ra4.
37. Biller A, Badde S, Nagel A, Neumann JO, Wick W, Hertenstein A, et al. Improved brain tumor classification by sodium MR imaging: prediction of IDH mutation status and tumor progression. AJNR Am J Neuroradiol 2016;37:66–73.
38. Hartmann C, Hentschel B, Wick W, Capper D, Felsberg J, Simon M, et al. Patients with IDH1 wild type anaplastic astrocytomas exhibit worse prognosis than IDH1-mutated glioblastomas, and IDH1 mutation status accounts for the unfavorable prognostic effect of higher age: implications for classification of gliomas. Acta Neuropathol 2010; 120:707–18.
39. van den Bent MJ, Dubbink HJ, Marie Y, Brandes AA, Taphoorn MJ, Wesseling P, et al. IDH1 and IDH2 mutations are prognostic but not predictive for outcome in anaplastic oligodendroglial tumors: a report of the European organization for research and treatment of cancer brain tumor group. Clin Cancer Res 2010;16:1597–604.
40. Yan H, Parsons DW, Jin G, McLendon R, Rasheed BA, Yuan W, et al. IDH1 and IDH2 mutations in gliomas. N Engl J Med 2009;360:765–73.
41. Parsons DW, Jones S, Zhang X, Lin JC, Leary RJ, Angenendt P, et al. An integrated genomic analysis of human glioblastoma multiforme. Science 2008;321:1807–12.
42. Beiko J, Suki D, Hess KR, Fox BD, Cheung V, Cabral M, et al. IDH1 mutant malignant astrocytomas are more amenable to surgical resection and have a survival benefit associated with maximal surgical resection. Neuro-oncology 2014;16:81–91.
43. Kawaguchi T, Sonoda Y, Shibahara I, Saito R, Kanamori M, Kumabe T, et al. Impact of gross total resection in patients with WHO grade III glioma harboring the IDH 1/2 mutation without the 1p/19q co-deletion. J Neuro-oncol 2016;129:505–14.
44. Asari S, Makabe T, Katayama S, Itoh T, Tsuchida S, Ohmoto T. Assessment of the pathological grade of astrocytic gliomas using an MRI score. Neuroradiology 1994;36:308–10.
45. Pope WB, Sayre J, Perlina A, Villablanca JP, Mischel PS, Cloughesy TF. MR imaging correlates of survival in patients with high-grade gliomas. AJNR Am J Neuroradiol 2005;26:2466–74.
46. Carrillo JA, Lai A, Nghiemphu PL, Kim HJ, Phillips HS, Kharbanda S, et al. Relationship between tumor enhancement, edema, IDH1 mutational status, MGMT promoter methylation, and survival in glioblastoma. AJNR Am J Neuroradiol 2012;33:1349–55.
47. Tay KL, Tsui A, Phal PM, Drummond KJ, Tress BM. MR imaging characteristics of protoplasmic astrocytomas. Neuroradiology 2011;53:405–11.
48. Babu R, Bagley JH, Park JG, Friedman AH, Adamson C. Low-grade astrocytomas: the prognostic value of fibrillary, gemistocytic, and protoplasmic tumor histology. J Neurosurg 2013;119:434–41.
49. Bai H, Harmanci AS, Erson-Omay EZ, Li J, Coskun S, Simon M, et al. Integrated genomic characterization of IDH1-mutant glioma malignant progression. Nat Genet 2016;48:59–66.
50. Johnson BE, Mazor T, Hong C, Barnes M, Aihara K, McLean CY, et al. Mutational analysis reveals the origin and therapy-driven evolution of recurrent glioma. Science 2014;343:189–93.
51. Wakimoto H, Tanaka S, Curry WT, Loebel F, Zhao D, Tateishi K, et al. Targetable signaling pathway mutations are associated with malignant phenotype in IDH-mutant gliomas. Clin Cancer Res 2014;20:2898–909.

Published OnlineFirst July 27, 2017; DOI: 10.1158/1078-0432.CCR-17-0560

Clinical Cancer Research

T2–FLAIR Mismatch, an Imaging Biomarker for IDH and 1p/19q Status in Lower-grade Gliomas: A TCGA/TCIA Project

Sohil H. Patel, Laila M. Poisson, Daniel J. Brat, et al.

Clin Cancer Res 2017;23:6078-6085. Published OnlineFirst July 27, 2017.